

X-ray powder diffraction at the XRD1 beamline at LNLS

A. M. G. Carvalho,^{a*} D. H. C. Araújo,^a H. F. Canova,^a C. B. Rodella,^a
D. H. Barrett,^a S. L. Cuffini,^b R. N. Costa^b and R. S. Nunes^c

^aLaboratório Nacional de Luz Síncrotron, CNPEM, Campinas, SP 13083-970, Brazil, ^bICT, UNIFESP, São José dos Campos, SP 12231-280, Brazil, and ^cUnidade Acadêmica de Física, UFCG, Campina Grande, PB 58429-900, Brazil.
*Correspondence e-mail: alexandre.carvalho@lnls.br

Received 31 March 2016

Accepted 5 August 2016

Edited by I. Schlichting, Max Planck Institute for Medical Research, Germany

Keywords: X-ray diffraction; beamline; bending magnet.

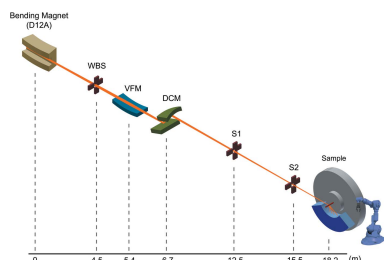
Various upgrades have been completed at the XRD1 beamline at the Brazilian synchrotron light source (LNLS). The upgrades are comprehensive, with changes to both hardware and software, now allowing users of the beamline to conduct X-ray powder diffraction experiments with faster data acquisition times and improved quality. The main beamline parameters and the results obtained for different standards are presented, showing the beamline ability of performing high-quality experiments in transmission geometry. XRD1 operates in the 5.5–14 keV range and has a photon flux of 7.8×10^9 photons s^{-1} (with 100 mA) at 12 keV, which is one of the typical working energies. At 8 keV (the other typical working energy) the photon flux at the sample position is 3.4×10^{10} photons s^{-1} and the energy resolution $\Delta E/E = 3 \times 10^{-4}$.

1. Introduction

The XRD1 beamline at the Brazilian Synchrotron Light Laboratory (LNLS) is a dedicated X-ray diffraction beamline (Cusatis *et al.*, 1998) in operation since 1998. The beamline is installed at the D12B bending magnet (1.67 T) and operates in the 5.5–14 keV range.

This beamline was upgraded recently. The mechanical stress on the optical elements and floor instabilities began causing beam stability problems as well as affecting the repeatability of the monochromator positions. Furthermore, user requirements for *in situ* powder diffraction experiments and faster detection speeds meant that the X-ray Powder Diffraction beamline (XPD) was becoming increasingly congested. The XRD1 diffractometer did not allow for easy installation of cell reactors and fast detection systems based on a set of linear detectors. Furthermore, the heavy detection system, which included a metallic casing, also gave problems. These limitations were the driving force for the beamline upgrade that began in 2011. Increasing beam instabilities led the LNLS to undertake a comprehensive restructuring of the optical hutch, including the construction of an independent concrete slab below the mirror and monochromator. Furthermore, the mechanics inside the monochromator were completely changed as well as the replacement of the two monochromator crystals (Canova *et al.*, 2014).

Commissioning tests of the optical elements showed that XRD1 gave a similar performance of photon flux at the sample position, energy resolution, motor repeatability and beam stability as the XPD beamline but with the advantage of a more spacious experimental hutch. Thus, the renovation continued to the experimental hutch with the installation of a



three-circle heavy-duty Newport diffractometer in 2013. The new diffractometer allows for faster measurements when combined with the MYTHEN 24K system from Dectris[®] (MYTHEN, 2014), and a robotic arm for rapid automated sample changing. Moreover, in 2014, a second experimental hutch was opened after the first hutch of XRD1. Both use the same X-ray beam and operate alternately. The second end-station (named XTMS) has a heavy-duty Huber diffractometer installed inside a thermo-mechanical simulator (Gleeble[®] Synchrotron system). The main goal of this facility is to perform structural studies on bulk metallic and non-metallic samples during thermic and/or mechanical tests (XTMS, 2015). The parameters of the XTMS end-station, which is not used for X-ray powder diffraction, will not be discussed in the present work.

The commissioning of the first end-station of the XRD1 beamline is now complete and optimized for structural characterization by X-ray diffraction experiments in Debye–Scherrer geometry, *i.e.* transmission mode of low-absorption materials. Samples are placed in glass or quartz capillaries for X-ray diffraction analyzes. Due to the relatively low energy of the beamline, sample thickness, particle size and sample packing have to be determined to optimize X-ray transmission. In general, low-absorption materials such as pharmaceuticals, ceramics, biomass, clays, catalysts and soils can be studied at XRD1. Carvalho *et al.* (2016) showed that it is also possible to obtain high-quality data for high-absorption materials using capillaries in the same geometry, despite the relatively low energies of the beamline. Besides the fast-automated experiments at room temperature, it is also possible to perform measurements at temperatures ranging from 100 K and 1070 K using two different devices. In addition, a capillary cell reactor has been developed to allow controlled flow of gases and/or vapor through the samples and its commissioning is in progress.

2. Beamline overview

2.1. Beamline optics

The optical layout of the XRD1 beamline is shown schematically in Fig. 1. The source is a 1.67 T bending magnet of the LNLS ring operating at 1.37 GeV (Craievich & Rodrigues, 1997; Rodrigues *et al.*, 1998), with a typical initial average current around 250 mA and an 11 h lifetime (February 2016).

From the source, the beam passes through a set of home-made automated slits (identified as WBS in Fig. 1). The slits are independent and water-cooled. This set of slits has the main function of limiting the horizontal and vertical dimensions and divergence of the incident beam. The horizontal divergence of the beam is regulated by the horizontal slits, which are typically separated by 27.4 mm, resulting in a divergence of 6 mrad.

After passing through the white-beam slits, the beam reaches a ULE (ultra-low expansion) Rh-coated glass mirror, located at about 5.4 m from the source, inside the optical hutch. The mirror is used to focus/collimate the white beam

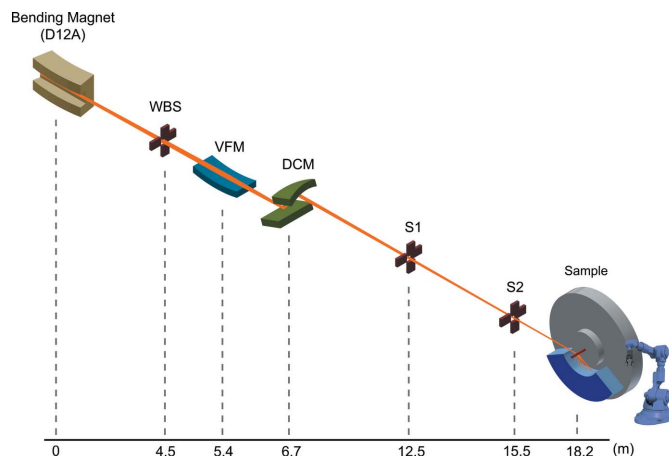


Figure 1

Schematic diagram of XRD1 beamline (excluding the second end-station). The diagram shows the bending magnet; white-beam slits (WBS); the vertical focusing mirror (VFM); the double-crystal monochromator (DCM); slits (S1 and S2); and the sample position on the heavy-duty diffractometer.

vertically, as well as filter off the high-energy photons. The mirror was fabricated with a curvature radius of 2.8 km. The cut-off energy of the photons is ~ 15 keV and it is defined by the rhodium coating as well as the incident angle of the white beam on the mirror, which is about 3.7 mrad. The mirror dimensions are 750 mm \times 80 mm. The mirror is accommodated in a vacuum chamber produced in-house, under a pressure of $\sim 10^{-7}$ Pa. Three independent motors (with a Heidenhain encoder) allow the mirror position to be adjusted (height and vertical and horizontal angles). Another motor (with a potentiometer-like encoder) is used to bend the mirror. The position of this motor is read by a 12-bit LOCON board. Home-made software (*SPUGULO*) controls the mirror movements and positions.

Monochromatization of the X-ray beam is performed using a double-crystal Si (111) monochromator developed in-house. The first crystal is flat (80 mm \times 80 mm \times 3 mm) and is water-cooled. The second crystal is bent for sagittal focusing. The double-crystal monochromator is mounted over a disc-shaped goniometer under high vacuum ($\sim 10^{-5}$ Pa), located inside the optical hutch 6.7 m from the source. With this system, the incident angle of the white beam over the first crystal (θ_m) is determined with precision and provides good stability.

There are two other sets of slits (identified as S1 and S2 in Fig. 1) inside the first-end station that are used to define the beam size at the sample position. The first set, located 12.5 m from the source, are similar to the WBS, but not water-cooled. The second set, closer to the diffractometer (15.5 m from the source), are a compact set of automated slits (from ADC company).

2.2. Diffractometer, detection system and accessories

The XRD1 beamline is equipped with a three-circle N3050-P1 diffractometer from Newport[®] (Fig. 2), which is installed 18.2 m from the source. Its goniometer is based on a one-axis

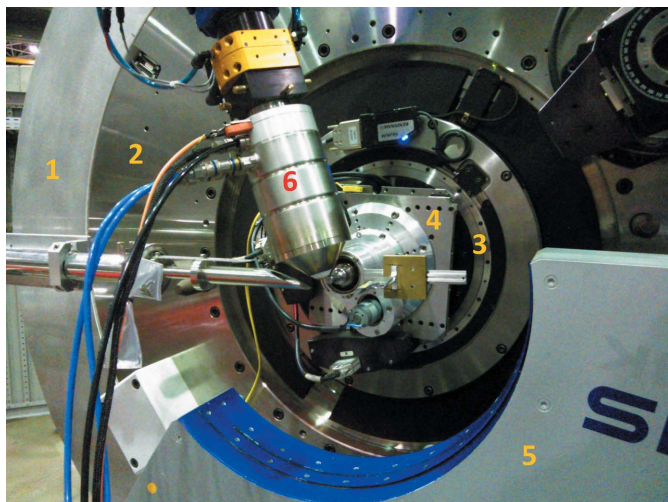


Figure 2
Photograph of the heavy-duty diffractometer at XRD1 beamline. (1) δ -circle; (2) 2θ -circle; (3) θ -circle; (4) XYZ sample positioner; (5) housing of the MYTHEN 24K system; (6) Gas Blower system.

object-positioning θ -circle and in line, centered on the same horizontal axis as the second- and third-circle detector holder. The 2θ - and δ -circles are designed to support a variety of heavy accessories such as detectors. Loadings of more than 100 kg for the 2θ -circle and 60 kg for the δ -circle are possible. The θ -circle is capable of supporting a 35 kg load, up to 20 kg with the open frame XYZ sample positioner. According to the manufacturer, the three circles have the same angular resolution (0.0001°), accuracy (0.001°) and zero position error (0.001°).

Although it is possible to use the θ - and 2θ -circles to perform X-ray powder diffraction in Bragg–Brentano geometry, in practice we have only been using the δ -circle, which supports the detectors for fast measurements in Debye–Scherrer geometry. Rigidly fixed onto the δ -circle is a housing for the MYTHEN 24K system (Dectris), from Dectris[®]. Inside the housing, there is a continuous flow of helium in order to reduce the absorption and scattering of the diffracted beam. The MYTHEN 24K system consists of 24 linear MYTHEN detectors installed 760 mm from the sample position, leading to a fixed angular resolution of 0.0037° . These detectors are $320\ \mu\text{m}$ thick and recommended to operate between 5 and 12.5 keV, according to the manufacturer. A complete description of the MYTHEN detectors was reported by Bergamaschi *et al.* (2010) and the instrumental profile of a MYTHEN detector in Debye–Scherrer geometry is discussed by Gozzo *et al.* (2010). These kinds of position-sensitive detectors have been used in different synchrotron facilities around the world, such as the Swiss Light Source (Bergamaschi *et al.*, 2010), Diamond Light Source (Thompson *et al.*, 2011) and Beijing Synchrotron Radiation Facility (Du *et al.*, 2016).

The angular calibration of the MYTHEN 24K system was performed using a well determined energy at 12 keV. In order to convert from channel number to 2θ angle, a series of

diffractometer center was calculated using the relation

$$R^i = \frac{p}{\tan(1/c^i)}, \quad (1)$$

where p is the pixel (channel) size, 0.05 mm, and c^i is the number of channels per degree in each module i . The corresponding angular value for each channel j inside each module i was obtained using the relation

$$\theta_j^i = \arctan\left[\frac{p(C_j^i - C_{\text{center}}^i)}{R^i}\right], \quad (2)$$

where C_j^i is the corresponding number of the channel j of the module i ; C_{center}^i is the central channel of each module. Finally, the angular offset of each module, θ_0^i , was obtained through a diffraction pattern of the LaB₆ NIST standard and the angular position refinement of the observed reflections in comparison with the calculated values. Therefore, the refined angular value for each channel j inside each module i is given by

$$\theta_j^i = \theta_j'^i + \theta_0^i. \quad (3)$$

The flat-field correction for the detectors was performed by the manufacturer.

At the XRD1 beamline, it is possible to perform X-ray powder diffraction experiments as a function of temperature. We have been using two different devices for variable temperature measurements: from 100 K up to 460 K, using the Cryojet5[®] (OXFORD Instruments); from room temperature to 1070 K, using the Gas Blower GSB 1300 (FMB Oxford) (see Fig. 2). According to the manufacturers, the working temperature ranges are larger. Nevertheless, we have limited these ranges after appropriate calibrations were conducted.

In order to increase the efficiency of the beamline during measurements, we have installed a robotic arm (Yaskawa-Motoman) to change samples quickly and automatically. This robotic arm is also used to hold both Cryojet5[®] and Gas Blower systems when performing measurements as a function of temperature.

2.3. Beamline parameters and performance

The photon flux at the sample position was measured at different X-ray wavelengths (Fig. 3) using a silicon photodiode (model AXUV-20HE1). The current from the photodiode was measured using a picoammeter (Keithley 6485). The maximum photon flux is about 3.8×10^{10} photons s^{-1} at 1.771 Å (7 keV), at 100 mA. Comparing with the results obtained in 2013, reported by Canova *et al.* (2014), we observe that the photon flux has been increased, mainly at higher wavelengths. Generally, the wavelength is kept at 1.033 Å (12 keV), unless it is necessary to perform resonant X-ray

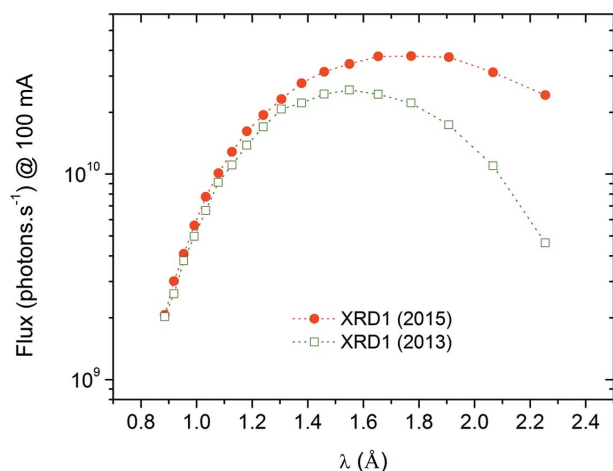


Figure 3
Photon flux at the sample position as a function of the X-ray wavelength. The data obtained in 2013 were reported by Canova *et al.* (2014).

diffraction experiments or to avoid fluorescence from specific atoms. At this wavelength, the photon flux is about 7.8×10^9 photons s^{-1} , at 100 mA. The beam is focused on the sample position with a size of 2.0 mm (horizontal) and between 0.6 and 0.7 (vertical), depending on the energy. These and other information are listed in Table 1.

The vertical size (FWHM) of the X-ray beam was determined by translating a silicon single-crystal across the beam at the sample position. The section of the beam not blocked by the crystal was measured by an ionization chamber. We observe that the vertical size of the beam has a minimum value at 15% curvature of the mirror (Fig. 4).

In order to determine the wavelength resolution of the X-ray beam with $\lambda = 1.54877(4)$ Å, rocking curves of the (111) and (333) reflections of a silicon single-crystal were recorded for different curvatures of the mirror. The wavelength resolution is evaluated using the following relation (Ferreira *et al.*, 2006),

Table 1
XRD1 information.

| | |
|-----------------------------|--|
| Beamline name | XRD1 |
| Source type | Bending magnet |
| Monochromator | Si(111) double-crystal |
| Mirror | Rh-coated |
| Energy range | 5.5–14 keV |
| Photon flux | 7.8×10^9 photons s^{-1} at 12 keV |
| (photons s^{-1} @ 100 mA) | 3.4×10^{10} photons s^{-1} at 8 keV |
| Beam size (focused) | 2.0 mm (horizontal) |
| | 0.6–0.7 (vertical) |
| Beam divergence | 116 μ rad (vertical) (unbent mirror) |
| (at the sample position) | |
| Resolution ($\Delta E/E$) | 3×10^{-4} at 8 keV |
| Diffractometer | Three-circle N3050-P1 diffractometer from Newport [®] |
| Detector | MYTHEN 24K from Dectris [®] |
| Temperature range | 100–1070 K |
| (at the sample) | |

$$\frac{\Delta\lambda}{\lambda} = \frac{\Delta E}{E} = \left\{ \frac{(w_{333}^2 - w_{111}^2) - (w_{D333}^2 - w_{D111}^2)}{[\tan(\theta_m) - \tan(\theta_2)]^2 - [\tan(\theta_m) - \tan(\theta_1)]^2} \right\}^{1/2}, \quad (4)$$

where w_{111} and w_{333} are the widths of the rocking curves; w_{D111} and w_{D333} are the theoretical Darwin widths of the (111) and (333) reflections, respectively, of the silicon crystal used; θ_1 and θ_2 are the angles of the (111) and (333) reflections, respectively; θ_m is the monochromator angle. At 8 keV, the theoretical Darwin widths for silicon are $w_{D111} = 6.79$ arcsec and $w_{D333} = 2.03$ arcsec. In Fig. 4, we observe that the variation of the wavelength resolution with the curvature of the mirror is almost linear. Since the best resolution is achieved with the smallest curvature of the mirror, we keep this condition during experiments.

X-ray powder diffraction measurements were conducted on NIST standard reference materials (SRM): Si (SRM 640d), Al_2O_3 (SRM 676a) and LaB_6 (SRM 660b). The LaB_6 standard was diluted in corn starch (LaB_6 34% wt and corn starch 66% wt) in order to reduce the X-ray absorption. The SRMs were placed inside 0.3 mm-diameter borosilicate capillaries, which are the thinnest capillaries used at XRD1 beamline. The capillaries are fixed in ferromagnetic stainless steel holders. Each capillary holder is fitted with a magnetic tip attached to the three-circle diffractometer. This magnetic tip is able to rotate, spinning the sample (~ 300 r.p.m.) during measurements. The measurements were conducted using the standard operating conditions (parameters) of the beamline: minimum curvature of the mirror; beam size of ~ 2.0 mm \times 0.7 mm at the sample position; MYTHEN 24K. Two different wavelengths were used, 1.54877 (4) Å (8 keV) and 1.03324 (3) Å (12 keV), keeping the temperature at 296 (1) K. Representative Bragg peaks of each diffraction pattern were fitted with a pseudo-Voigt function, using the software *PyMca* (Version 5.0.3). The linewidths (FWHM) of the peaks of each standard sample as a function of 2θ (Fig. 5) were fitted with the Caglioti function (Caglioti *et al.*, 1958),

$$FWHM = (U \tan^2 \theta + V \tan \theta + W)^{1/2}. \quad (5)$$

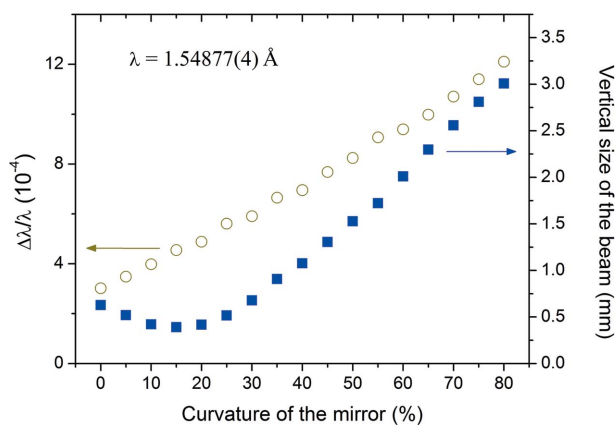


Figure 4
Wavelength resolution and vertical size of the beam at the sample position as functions of the curvature of the mirror [0% and 100% correspond to minimum (3.5 km) and maximum (1.4 km) allowed curvature, respectively].

Table 2

 Agreement R -factors and wavelength values from the structural refinements of NIST standards Si and Al_2O_3 measured at 12.0 keV.

 U , V and W parameters used to fit the experimental linewidths of these standards (Fig. 5) are also listed.

| Standards | R_{exp} | R_{wp} | λ (Å) | $\lambda = 1.54877$ Å | | | $\lambda = 1.03324$ Å | | |
|------------------------------------|------------------|-----------------|---------------|-----------------------|----------|----------|-----------------------|----------|----------|
| | | | | U | V | W | U | V | W |
| Si (SRM 640d) | 4.82 | 10.32 | 1.033303 (1) | 0.001983 | 0.000182 | 0.000759 | 0.002774 | 0.000002 | 0.000415 |
| Al_2O_3 (SRM 676a) | 3.08 | 6.75 | 1.033167 (2) | 0.002906 | 0.001209 | 0.002886 | 0.004289 | 0.000548 | 0.001102 |

The parameters U , V and W used to obtain the fits shown in Fig. 5 are listed in Table 2. The largest contribution for the linewidths of the standard Si comes from the Gaussian part of the pseudo-Voigt function. Since this standard is claimed to have no microstrain (NIST, 2010), its linewidths may be taken as good estimates of the instrumental resolution (including the contribution of the 0.3 mm-diameter capillary).

The X-ray powder diffraction patterns of the standards obtained at 12.0 keV were analyzed using the Rietveld method (Rietveld, 1969) and *TOPAS* (Version 4.1) software. The agreement R -factors for Si and Al_2O_3 obtained from the Rietveld refinements are listed in Table 2. The measured and calculated X-ray diffraction profiles for the NIST standard Al_2O_3 are shown in Fig. 6. The inset shows five consecutive reflections with more detail: $(\bar{3}42)$, $(\bar{1}38)$, (0210) , $(00\bar{1}2)$ and $(\bar{1}44)$ at $2\theta \simeq 54.62^\circ$, 54.70° , 56.07° , 56.99° and 57.24° , respectively. The differences between the calculated and observed profiles for the three standard samples are relatively small (the fittings are very satisfactory), as exemplified for Al_2O_3 (Fig. 6). The refinement of the LaB_6 standard diluted in corn starch resulted in the agreement R -factors $R_{\text{exp}} = 4.47$ and $R_{\text{wp}} = 9.09$.

The influence of the capillary diameter on the linewidths can be observed in Fig. 7(a). The NIST standard Si (SRM 640d) was measured inside capillaries with three different diameters: 0.3, 0.5 and 0.7 mm. These measurements were executed off the optimal conditions of resolution. It is easy to notice that the linewidth becomes larger with the size of the capillaries in a non-linear way. The widths of the observed

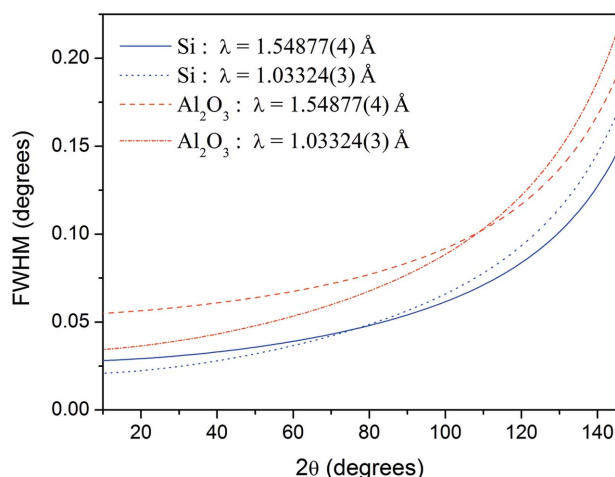
peaks are dominated by the contribution of large capillaries. In Fig. 7(b) we show the experimental data and the refinement results for two silicon reflections at high angles. The data were obtained using a 0.3 mm-diameter capillary. Comparing with the results obtained on I11 beamline at Diamond Light Source (Thompson *et al.*, 2011), we noticed that, for a similar angle range, the linewidths from our results are about 54% larger. Nevertheless, at low angles, the linewidths are small enough to solve the great majority of the scientific cases related to X-ray powder diffraction submitted to LNLS nowadays.

3. Facility access

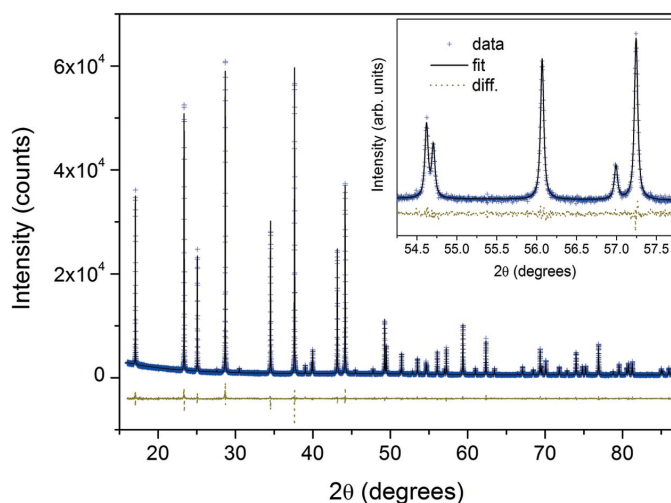
Access to the Brazilian Synchrotron Light Laboratory is merit-based. Researchers submit scientific proposals to XRD1 beamline once a semester. All proposals are independently peer-reviewed and scored by an external scientific committee. The execution of the accepted proposals is always (and only) in the following semester. In the near future, it will be possible to conduct experiments at XRD1 remotely. Further information can be requested from the beamline coordinator by email (alexandre.carvalho@lnls.br).

4. Conclusions

The commissioning of the first end-station of XRD1 beamline is now complete and we are able to conduct high-quality X-ray powder diffraction experiments. This is optimized for experiments with low-absorption materials (such as medicines) in


Figure 5

Bragg peak widths (full width at half-maximum in 2θ) as a function of 2θ for the standards Si and Al_2O_3 . The lines are fits for the experimental FWHM values.


Figure 6

Observed and calculated X-ray powder diffraction intensities for Al_2O_3 reference powder (NIST SRM 676a). Acquisition time: 140 s.

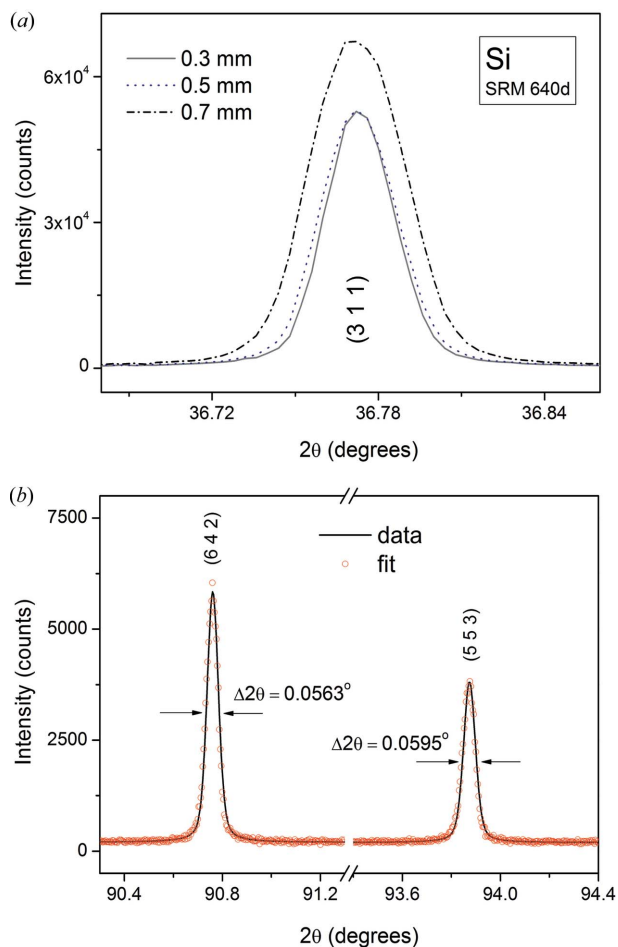


Figure 7
 (a) Reflection (311) of NIST standard Si (SRM 640d) analyzed inside capillaries with three different diameters (0.3, 0.5 and 0.7 mm). (b) Reflections (642) and (553) of Si obtained inside a 0.3 mm-diameter capillary.

powder form. The instrumental resolution is sufficient to solve the great majority of the scientific cases related to X-ray powder diffraction submitted to LNLS nowadays. The devices for variable-temperature measurements are operating well. For low-absorption materials, we obtain good quality data using either dynamic or isothermal processes. For superior results with high-absorption materials, we suggest diluting

them before the measurements. A capillary reactor cell has been developed and its commissioning is in progress. This and other developments and improvements will be transferred to the new X-ray powder diffraction beamline (Paineira) at the new fourth-generation Brazilian synchrotron (Sirius).

Acknowledgements

We thank all the technicians and scientists that worked to build and improve the XRD1 beamline. We also acknowledge LNLS and the financial support from FAPESP and CNPq.

References

Bergamaschi, A., Cervellino, A., Dinapoli, R., Gozzo, F., Henrich, B., Johnson, I., Kraft, P., Mozzanica, A., Schmitt, B. & Shi, X. (2010). *J. Synchrotron Rad.* **17**, 653–668.
 Caglioti, G., Paoletti, A. & Ricci, F. P. (1958). *Nucl. Instrum.* **3**, 223–228.
 Canova, H., Fontoura, A., Neuenschwander, R. T., Diaz, B. & Rodella, C. B. (2014). *J. Phys. Conf. Ser.* **493**, 012004.
 Carvalho, A. M. G., Nunes, R. S. & Coelho, A. A. (2016). arXiv: 1608.00565 [physics.ins-det].
 Craievich, A. F. & Rodrigues, A. R. D. (1997). *Braz. J. Phys.* **27**, 417–424.
 Cusatis, C., Kobayashi Franco, M., Kakuno, E., Giles, C., Morelhão, S., Mello, V. & Mazzaro, I. (1998). *J. Synchrotron Rad.* **5**, 491–493.
 Du, R., Cai, Q., Chen, Z., Gong, Y., Liu, H. & Wu, Z. (2016). *Instrum. Sci. Technol.* **44**, 1–11.
 Ferreira, F. F., Granado, E., Carvalho Jr, W., Kycia, S. W., Bruno, D. & Droppa Jr, R. (2006). *J. Synchrotron Rad.* **13**, 46–53.
 Gozzo, F., Cervellino, A., Leoni, M., Scardi, P., Bergamaschi, A. & Schmitt, B. (2010). *Z. Kristallogr.* **225**, 616–624.
 MYTHEN (2014). *MYTHEN Microstrip X-ray Detectors*, https://www.dectris.com/tl_files/root/products/mythen_family/MYTHEN%20Brochures/MYTHEN_8Seiter_Jun2014_final_web.pdf.
 NIST (2010). *SRM 640d; Silicon Powder Line Position and Line Shape Standard for Powder Diffraction*. National Institute of Standards and Technology, Gaithersburg, MD, USA.
 Rietveld, H. M. (1969). *J. Appl. Cryst.* **2**, 65–71.
 Rodrigues, A. R. D., Craievich, A. F. & Gonçalves da Silva, C. E. T. (1998). *J. Synchrotron Rad.* **5**, 1157–1161.
 Thompson, S. P., Parker, J. E., Marchal, J., Potter, J., Birt, A., Yuan, F., Fearn, R. D., Lennie, A. R., Street, S. R. & Tang, C. C. (2011). *J. Synchrotron Rad.* **18**, 637–648.
 XTMS (2015). *XTMS Experimental Station*, <http://lnnano.cnpem.br/laboratories/cpm/facilities/xtms/>.